EXPERIMENTAL DETERMINATION OF THE PT K EDGE

K-FACTOR FOR NANOPARTICLE ORDER-

DISORDER TRANSITION ANALYSIS

by

Amy Jackson

Submitted to Brigham Young University in partial fulfillment

of graduation requirements for University Honors

Department of Physics and Astronomy

Brigham Young University

August 2012

Advisor: Richard Vanfleet   Honors Representative: Sean Warnick

Signature:_____   Signature:_____

ABSTRACT

EXPERIMENTAL DETERMINATION OF THE PT K EDGE

K-FACTOR FOR NANOPARTICLE ORDER-

DISORDER TRANSITION ANALYSIS

Amy Jackson

Department of Physics and Astronomy

Bachelor of Science

Analysis of the order-disorder transition in metallic alloy nanoparticles is a vital yet challenging area of ongoing research. Current methods of sample preparation and diffraction analysis were used to analyze samples of 5-10 nm FePt nanoparticles with the aim of evaluating and calculating new standards for energy dispersive X-ray spectroscopy (EDS) analysis. Through comparison with Rutherford backscattering spectrometry (RBS) data, a Pt L edge *k*-factor of 4.291 ± 0.272 was obtained for use in further research into FePt and NiFePt nanoparticle ordering in BYU's electron microscopy facility.

TABLE OF CONTENTS

List of Figures and Tables

CHAPTER 1

Introduction

1.1 Order-disorder phase transition in metallic alloys

The order-disorder phase transition of intermetallic alloys has been extensively researched as an interesting and useful property of those widely utilized materials both in academia and industry. Intermetallic alloys often form a face-centered cubic (fcc) crystal structure, in which atoms are arranged in parallel planes, with a randomized probability of an atom of a given element being located at each lattice site. Such binary alloys as AuCu and FePt can also form a phase in which the atoms order themselves into near-homogeneous planes alternating by element (i.e. one plane of Au atoms, one plane of Cu atoms, etc.) [1]. For compositions close to 50/50 and temperatures below a material-specific threshold, the transition from the unordered fcc A1 phase to this ordered face-centered tetrahedral (fct) $L1_0$ phase is even energetically preferable.

      This research focuses on the prototypical ferromagnetic $L1_0$ material, iron-platinum (FePt), which in bulk can form the ordered $L1_0$ phase for Fe atomic content from 35% to 60% and temperatures beneath 1300°C (see figure 1). This ordered phase has magnetic properties with potential applications in high-performance permanent magnets and in data recording media [2] [3].
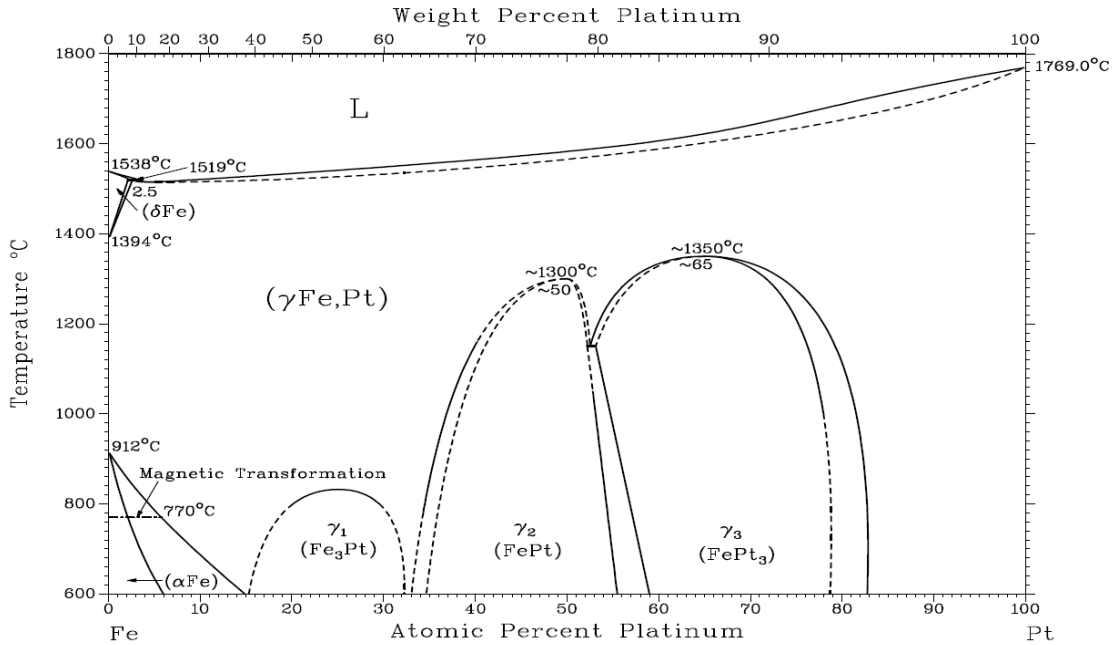
Figure 1: *Phase diagram showing melting point and order-disorder transitions for FePt in bulk materials; the L1$_0$ phase is represented by the γ_2 (FePt) region [4]*

1.2 Demand for research in nanomaterials

Industry continues to push the boundaries in the field of nanotechnology, but despite the wealth of knowledge concerning bulk order-disorder transitions, the order-disorder transition of nanomaterial metallic alloys has largely escaped the attention of the global research community. Even theoretical and computational models are not as developed as one could wish. Research done on the variations in melting points and Curie temperatures between bulk and nanomaterials indicate that as particle size decreases, these transition temperatures also decrease, and the transition becomes more gradual and less abrupt [2]. By analogy, the order-disorder transition should display similar behavior, an expectation supported by what computational models are available [3], but very little experimental work has been performed to date.

Considering especially L1$_0$ materials' potential applications in data storage,

2

experimental verification of these postulates is essential. The hard disk drives used in countless modern devices have a data storage capacity limited by the physical size of their information bits, which must be magnetically anisotropic to be effective. Conventional bits are composed of dozens of coupled metallic alloy grains, but improved areal storage density could be achieved with smaller $L1_0$ grains, provided those grains remain ordered over a range of temperatures at nanoparticle size [2], behavior which has yet to be experimentally verified. Without a better understanding of the order-disorder transition behavior of intermetallic alloy nanoparticles, ignorance of the properties of these materials limits both scientific and technological progress.

1.3 Considerations in nanoparticle research

The three factors which have the greatest impact on nanoparticle ordering in intermetallic alloys are particle size, composition, and temperature [3]. Focusing only on particles from 3-10 nm in size introduces immediate experimental difficulties; exploration on such a scale requires the use of electron microscopes. After thus controlling for particle size the remaining factors of interest are temperature and composition.

Temperature plays a role in nanoparticle ordering in two ways. First, anneals at various temperatures provide the kinetics necessary for bimetallic thin films to form nanoparticles of the desired size. Once nanoparticles have formed, they require additional kinetics to overcome the potential barrier and transition from their as-deposited, disordered A1 phase to their ordered $L1_0$ phase. Examination of the second role temperature plays is beyond the scope of this thesis, but will be the focus of further investigation using the results obtained here. As an ordered particle's temperature is

3

ramped up, it will eventually exceed the order-disorder transition temperature and disorder. For this project, particles were examined at room temperature or below, thus staying well below the order-disorder transition temperature.

Accurate measurements of sample composition are vital to a full understanding of order-disorder behavior, since the order-disorder transition temperature is actually a function of particle composition (as demonstrated in figure 1). To build a cohesive picture of order-disorder behavior, knowing particles' specific compositions is thus imperative. Rutherford backscattering spectrometry (RBS) is useful as an initial measurement of the samples' general chemical compositions, but cannot be used on the small scale which nanoparticle research requires. A more appropriate method is energy dispersive X-ray spectroscopy (EDS), but that too has limitations, particularly computationally. EDS analysis uses theoretical atomic models and detector-dependent numerical factors called '*k*-factors' to quantify the chemical composition of nanomaterial samples based on the number of characteristic X-rays emitted (within a certain energy range) from the samples. The *k*-factors are fairly accurate for the K edges of most elements, but have very large uncertainties for the L and M edges [5]. The Fe K edge is within the EDS detector range, and is known to ±5% confidence, but the Pt K edge is out of range, leaving the more difficult L edge (which is only known to ±15% confidence) from which to measure Pt content. Thus, to track nanoparticle composition with greater accuracy, the focus of this thesis is on experimentally determining the BYU system's *k*-factor for the Pt L edge from the ratio between the Fe K edge *k*-factor and the Pt L edge *k*-factor through analysis of FePt nanoparticles.

1.4 Development of the project

The initial direction of this project was to track nanoparticle ordering in NiFePt particles up to and beyond the order-disorder transition temperature in the TEM, but execution of that experiment requires already-ordered particles. From previous work, my advisor knew that FePt nanoparticles have a very strong driving force to order at room temperature, so to get an idea of what kind of ordering was possible we started looking at FePt samples which had been annealed at temperatures up to 600°C, but found no evidence of ordering. Previous work indicated that those anneals may not have been energetic enough to get the particles to order, so higher-temperature anneals for the particles were suggested.

Analysis of the FePt samples also revealed significant discrepancies between RBS measurements and EDS measurements of sample compositions. This discrepancy could stem from either a mistake in the EDS analysis (due to the inaccuracy of the Pt k-value for the L edge) or an actual change in composition during the anneal process (which had been observed in previous work with FePt nanoparticles [6]). Annealing more samples in a wet environment was suggested to control for anneal-driven compositional changes (the technique which had solved the problem in earlier projects).

These two factors together led to a request for samples wet annealed at 700°C and 800°C, again at 30 minutes each. When those arrived, ordering was found in the 800°C samples. The EDS measurements still differed significantly from the RBS values, thus began the process of calculating a new k-factor. In the course of that analysis, one of the RBS values from which we'd been working was discovered to be inaccurate; new RBS measurements were taken, and these were used for the final results presented here.

CHAPTER 2

Experimental Methods

2.1 Deposition and annealing

Colleagues at the University of Central Florida (UCF) prepared a range of samples of varying compositions at varying anneal temperatures. They co-sputtered FePt in thin film depositions from high purity Fe and Pt targets at five different power ratios (Pt held constant at 10 W for each, with Fe at 37W, 39W, 41W, 43W, and 45 W) onto silicon (Si) wafers with an amorphous silicon oxide (SiO_2) layer. They then measured the percentage composition of Fe and Pt in the thin film depositions through Rutherford backscattering spectrometry (RBS). The sputtered wafers were cleaved and pieces of each composition were annealed for 30 minutes at 400°C, 500°C, or 600°C to provide the kinetics necessary for nanoparticle formation and possible ordering (figure 2). These anneals were conducted in an argon and hydrogen "dry anneal" environment; Ar is an inert gas but inevitably introduces residual O_2 into the anneal environment, so the H_2 is present to reduce the Fe and prevent the formation of oxides in the sample.

As discussed at greater length later in this thesis, when additional pieces of each composition were later annealed at 700°C and 800°C, the new samples were annealed for 30 minutes in a "wet anneal" environment consisting of Ar and H_2 and water vapor. While the H_2 successfully prevented the formation of iron oxide, the iron became mobile enough in the hotter anneals to diffuse through the SiO_2 substrate. The added H_2O
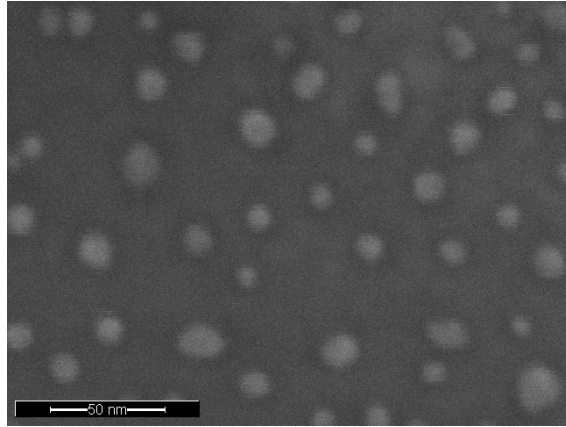
Figure 2: *SEM image of FePt nanoparticles on Si/SiO$_2$ substrate after 800°C wet anneal*

provided enough oxygen to fix the Fe on the sample surface, with the balance between the oxidization and reduction processes maintaining constant Fe composition through the annealing process.

Rather than referring to these sputtering and annealing series by composition (i.e. 53% Fe 47% Pt) which by the nature of the measurements has uncertainty attached to it, these series are referred to by their sputtering ratios for the remainder of this thesis (i.e. Fe39Pt10 or simply 39/10).

2.2 Sample preparation

In order to view nanoparticles in Brigham Young University's high-resolution Tecnai F20 Analytical Transmission Electron Microscope (TEM) the samples must be thinned to electron-transparency and mounted on TEM grids.

In the first part of this process, smaller samples (roughly 2-mm square) are cleaved from the prepared silicon wafers from UCF, cleaned in a 50/50 solution of Mr. Clean® and water, and rinsed in acetone and methanol. Cleaned samples are mounted on a tripod polisher with crystal bond mounting wax, with particle side to the glass surface.
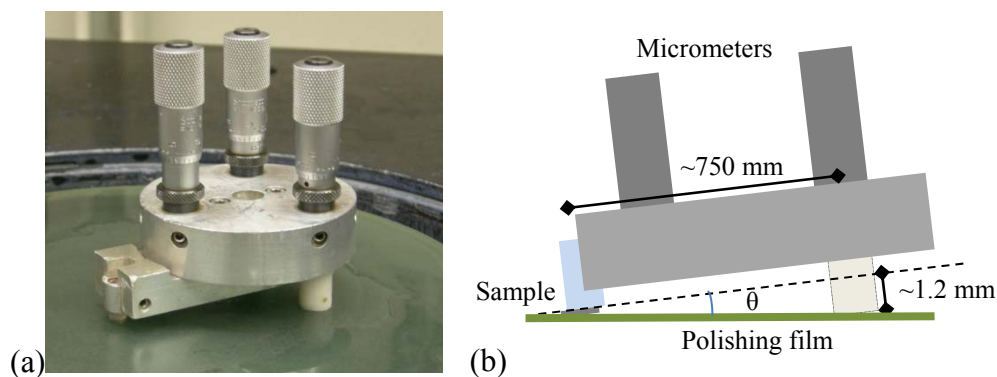
Figure 3: *Tripod polishing of a wedge sample and a schematic (not to scale) showing the positioning of the sample for a sufficiently small angle at the sample tip ($\theta \approx 0.0016$ radians)*

The back legs of the tripod polisher are set 1.2 mm higher than the surface of the glass rod, thus establishing a shallow angle to polish the sample into a wedge shape (figure 3b). Using successively finer-grade diamond lapping films (30 μm, 6 μm, 3 μm, 1 μm, 0.5 μm) and a colloidal silica suspension on a felt pad, the bulk of the Si substrate is polished away from the particles (figure 3a).

The colloidal silica phase of this polishing process is particularly impactful; if done improperly, colloidal silica particles can remain on the edge of the completed sample and interfere with TEM imaging, diffraction patterns, and EDS spectra. Colloidal silica particles can also get in between the sample and the glass rod, thus clearing the edge of the sample of particles, etching away material from particles, and otherwise rendering the sample useless. Two practices which help to avert such colloidal-silica-induced disasters are ensuring that the mounting wax layer between the sample and the glass is very thin and well adhered to the sample, and keeping the polishing pad during the colloidal silica polishing phase well lubricated to prevent vibrations in the sample. After colloidal silica, the sample is passed over a wet felt vel-cloth, which ideally removes any remaining colloidal silica particles or other debris from the sample prior to

mounting it.

Once a sample is sufficiently smooth and thin, it is freed from the tripod polisher in an acetone bath, rinsed in acetone and methanol, and mounted with M-Bond epoxy on 3-mm copper or platinum TEM grids (figure 4). The mounted sample is then heated on a hotplate at ~110°C for 30 minutes to cure the epoxy and reduce out-gassing in the TEM chamber.
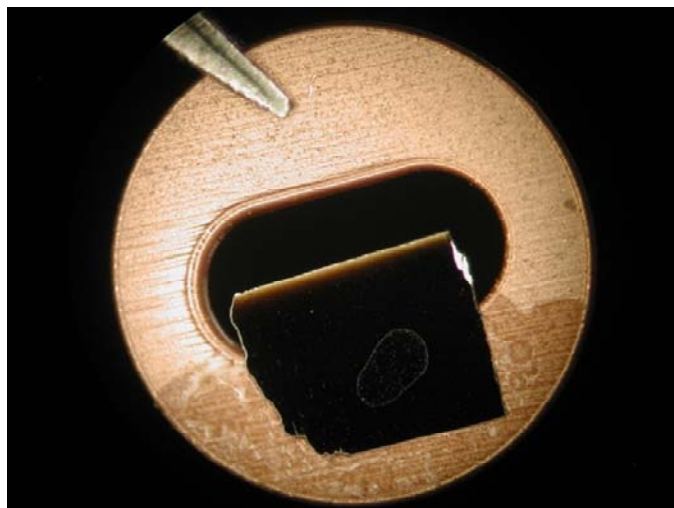
Figure 4: *Prepared wedge sample ready for TEM analysis. The copper washer has a diameter of 3 mm, tweezers are visible holding the sample at the top left, the orange-colored region of the sample at the tip is thin enough to exhibit Fresnel fringes.*

2.3 Diffraction analysis

Diffraction patterns from wedge samples in the TEM are obtained by passing the collimated electron beam through the thin tip of the sample and viewing the beam in a diffraction plane instead of an image plane. The atomic-level structure of nanoparticles and their silicon substrate is thus readily viewed and imaged in the diffraction mode of the TEM. Due to the structured crystal lattice of FePt even in a disordered state, the atomic planes will act as a diffraction grating from which the incident electron beam scatters in a predictable manner. Bragg's law describes this behavior, and in the small-

angle approximation (appropriate here due to the very small wavelength of TEM energy electrons and thus the small angle of electron scattering) yields:

$$m \, \lambda = 2 \, d \, \sin(\theta_b) \approx 2 \, d \, \tan(\theta_b) = 2 \, d \cdot \frac{R/_2}{L} \qquad\qquad 2.1$$

and thus $R \propto {}^{1}\!/_{d}$ \qquad\qquad 2.2

where λ is the wavelength of the diffracted wave, θ_b is the Bragg angle (which is half the angle from the direct beam to the mth diffraction peak), R is the physical distance between the mth peak and the central peak on the viewing screen, d is the spacing of the diffraction 'grating' – in this instance the d-spacing of the atomic planes in the nanoparticles – and L is the distance from the sample to the viewing screen.

Those diffraction peaks representing close-spaced 100 planar periodicity will be present in both the unordered fcc A1 phase and the ordered fct $L1_0$ phase. Since diffraction space is a reciprocal space to real space (Eq. 2.2) the more widely-spaced 001 periodicity of the $L1_0$ phase will generate closer-spaced diffraction peaks, corresponding to the element-alternating atomic planes (figure 5).
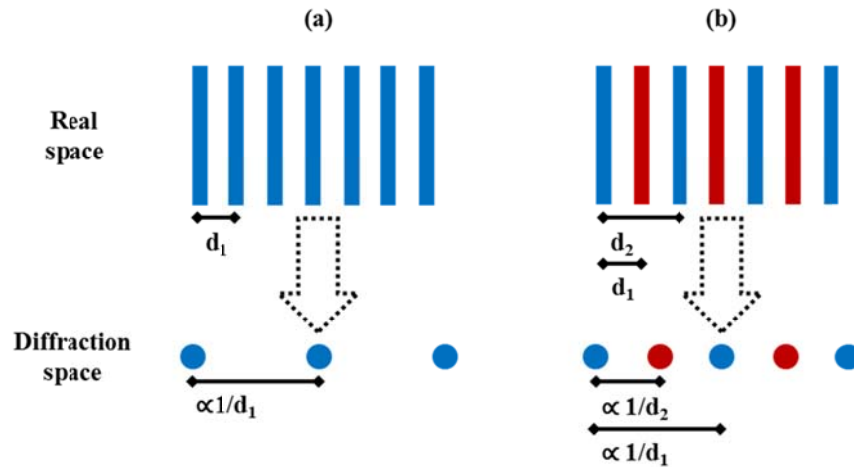
Figure 5: *Relationship between real space lattice d-spacing and diffraction peak spacing for (a) a random A_1 alloy (b) an ordered $L1_0$ alloy*

Individual metallic particles' diffraction patterns generally are grid-like, reflecting their crystalline structure. In this research, since the objective was simply obtaining evidence of ordering rather than quantifying the degree of ordering in particular particles, diffraction patterns were obtained from sample areas including many particles. In such a collection of nanoparticles, the different orientations of many particles generate many grid patterns rotated around the central peak, coincident with the direct beam, for an overall diffraction pattern in the form of a series of concentric rings. The radius of each ring thus corresponds to a particular d-spacing in the crystal structure of the particles present. The presence of rings at specific "ordering" radii verifies the ordering of the sample (figure 6), since ordered particles generate differently-spaced peaks than unordered particles (figure 5).
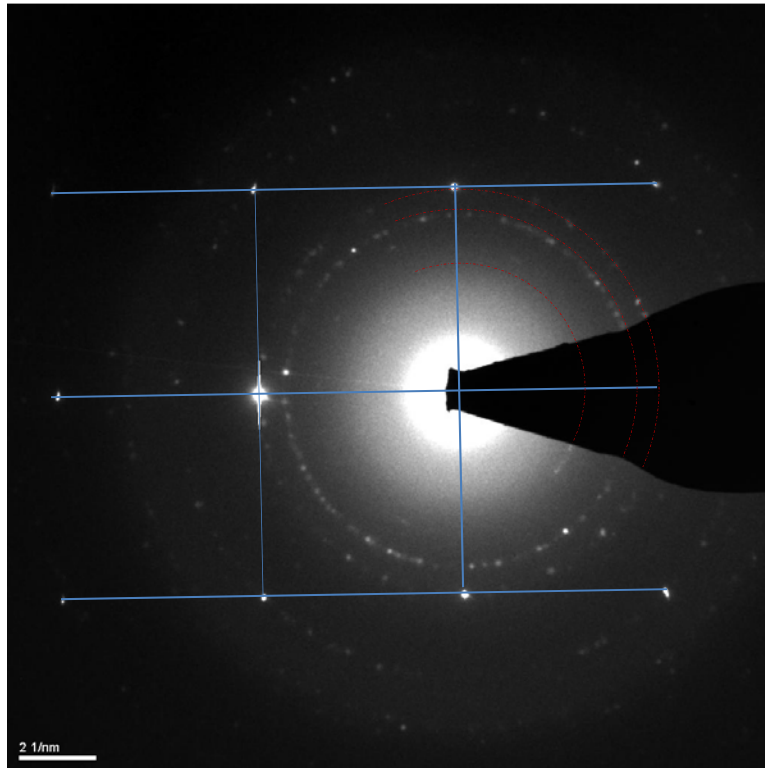
Figure 6: Nanoparticle diffraction pattern displaying the grid-like Si lattice structure as well as rings from the variously-oriented nanoparticles. The rings at the two larger indicated radii are expected for both ordered and disordered particles; the presence of diffraction peaks at the smaller radius indicates the presence of ordered particles.

11

As a matter of practicality, the closer to the tip of the sample that a diffraction pattern is obtained, the less the diffraction pattern of the Si substrate will interfere with viewing the diffraction pattern from the nanoparticles. Diffraction patterns from thicker regions of the sample, further back from the tip, are dominated by the strong Si scattering. When particles are accessible up to the very edge of a sample, the effect of the Si substrate can be completely eliminated, since only the amorphous SiO_2 remains supporting the particles at the very thinnest parts.

2.4 EDS Spectroscopy

EDS spectra measure the composition of samples in the TEM. In EDS analysis, the incident electron beam from the TEM interacts with the atoms of the sample to stimulate X-ray emission. The beam from the TEM electron gun excites inner electrons from the ground state of atoms in the sample, which leave electron holes for electrons in higher orbitals to drop down and fill. When higher-energy electrons drop down to lower energy levels, they emit discrete quantities of energy in the form of x-rays (figure 7) which are then counted and binned according to energy by the EDAX detector on BYU's F20 TEM. Since each element has a specific atomic structure, with discrete and unique electron shells, the energy of the detected X-rays corresponds to electron transitions between specific shells in specific elements [5]. The characteristic energies of interest in this investigation are the Fe K edge and the Pt L edge.
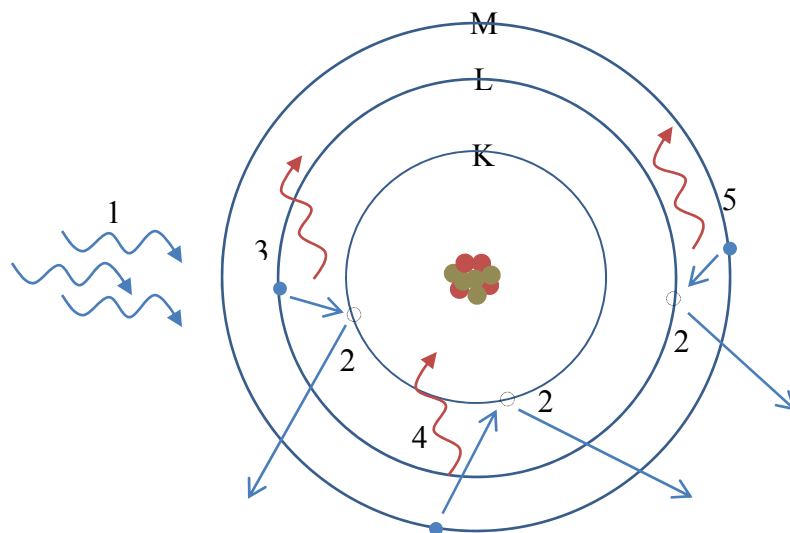
Figure 7: *In EDS, the incoming electron beam (1) knocks inner electrons from their orbitals (2) leaving electron holes which are filled when higher electrons emit characteristic X-rays to drop to a lower energy level (3: a K_α edge transition, 4: a K_β edge transition, 5: an L_α edge transition)*

Obtaining good-quality EDS spectra involves a balance between obtaining sufficient counts for a distinct spectrum and allowing the detector to record those counts with maximum efficiency. Too many total counts per second (cps) can damage the detector (BYU's EDAX has a recommended maximum of 50,000 cps) and increase detector artifacts in the spectrum, and too few counts take too long, with too little competition with the background to get the desired statistics.

To ensure a spectrum that is an accurate measurement of the sample's composition, the detector must pick up many times more counts in the edges of interest than from the background. The detector picks up a small but inevitable level of true background radiation in addition to higher, broadband background levels from the sample environment. These "bremsstrallung" X-rays arise from the bending of the electron path within the sample. The copper washer on which the sample is mounted also contributes a Cu K edge which can dominate the spectrum (figure 8). For each X-ray which registers,

the detector shuts down to integrate for a certain time period to determine the photon energy by integrating charge generation within the semiconductor active region of the detector. If more than one photon enters the detector during that time period (a consequence of high cps) the energy of that photon is incorrectly determined and artifacts in the spectra are generated. A commonly encountered artifact in this research was a peak at 3.68 keV which doesn't correspond to any elements in the sample, but does correspond to the absorption of two Si K edge (1.84 keV) photons [7] (figure 9). The measure of how long the detector is integrating as compared to total measurement time is known as the dead time ratio. This should be kept as low as possible to reduce detector artifacts, optimally from 10 to 20 percent, and must be balanced with speed of spectra collection to get sufficient statistics on the edges of interest.

Adjusting the detector cps can be achieved by increasing electron beam intensity (hitting the sample with more electrons via spot size and extraction voltage) or by moving the beam to a part of the sample which generates more X-rays (generally thicker areas, which have more matter and thus give electrons a better chance of exciting atoms as they pass through). This last method is effectively useless for this project's purposes, as the additional counts come from the thicker substrate rather than from the particles on the surface, which have uniform size over the entire sample. For similar reasons, when the electron beam is spread over a larger area, it is important to not spread the beam too far back from the thin edge of the sample, into thicker and thus less useful areas. Data for this research was taken at rates from 3,000 cps to 15,000 cps, depending on beam quality, sample quality, and time constraints on the researcher.
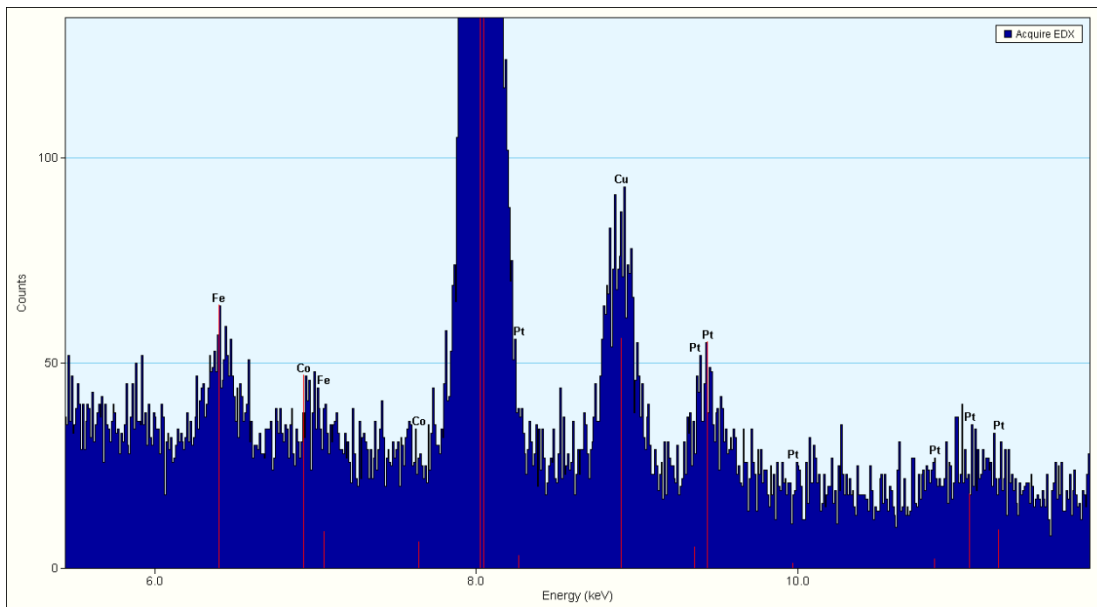
Figure 8: EDS from a 41/10 sample annealed at 400C, integrated over 90 s at 3500 cps. The Cu washer (Kα edge at 8.048 keV) and background bremsstrallung dominate this low-cps spectrum, generating considerable uncertainty in the accuracy of the counts for the Fe and Pt peaks, since they are scarcely distinguishable from background counts.
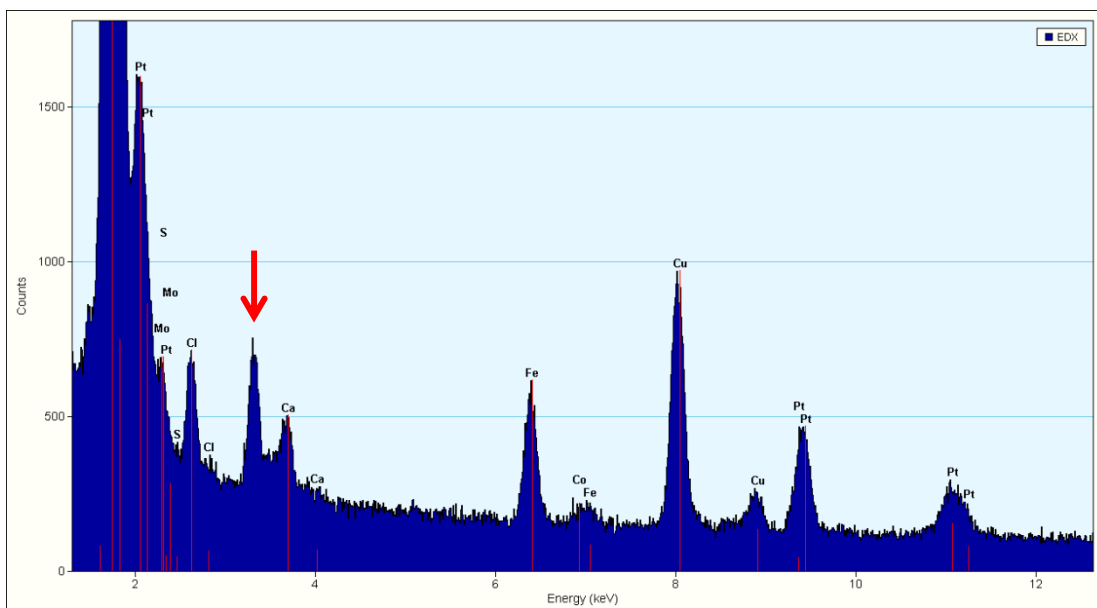
Figure 9: EDS from a 43/10 sample annealed at 800C, integrated over 60 s at 12000 cps. The cps rate was high enough to generate a false peak at 3.68 keV, double the Si K edge energy (1.84 keV, the right-most peak, large enough to be cut off in this view), but the Fe and Pt peaks are distinct.

15

Lower cps measurements can still yield accurate EDS spectra by compensating for the reduced count rate with increased integration times. This can increase the total background counts recorded, but as long as sample counts are still significantly greater than background, it's not a source of great concern. Integration times from 30 seconds to 120 seconds were used to obtain the spectra used in this research. A minimum of four EDS spectra from four separate locations on each sample were collected; these were later analyzed and averaged to calculate the Pt k-factor, as detailed in Chapter 4.

One consideration in taking the EDS spectra is associated with the construction of the TEM column; an iron-cobalt pole piece (part of the microscope's magnetic lenses) is situated such that it too undergoes stimulated X-ray emission under most beam conditions, thus the detector often picks up additional Fe and Co counts from this pole piece. This issue will be addressed in greater depth in the "Discussion and Analysis" section of this thesis.

CHAPTER 3

Experimental Results

3.1 Verification of Ordering

To explore the connection between composition, anneal temperature, and ordering, diffraction patterns were obtained from samples prepared by colleagues at UCF. It was impossible to obtain diffraction patterns from the first samples I prepared, as the samples themselves didn't meet the necessary criteria of retaining FePt nanoparticles to a colloidal-free sample edge. Once my sample preparation technique improved, I was able to examine all five samples (37/10, 39/10, 41/10, 43/10, 45/10) annealed at 600°C, but found no evidence of ordering (figure 10a). Similar analysis of the temperature-constant series at 500°C and at 400°C indicated that those particles were also not in the $L1_0$ phase. Since the RBS compositions were the desired range, and it was very unlikely that the order-disorder transition temperature would have dropped from 1300°C in bulk materials to 400°C or lower in nanoparticles, it was possible that the kinetics of the three anneals might have been insufficient for ordering. After consulting with my advisor, I decided to try samples annealed at higher temperatures, since previous research indicated that FePt nanoparticles require significant kinetics to transition from the A1 to the $L1_0$ phase.

The second set of FePt samples, prepared at higher temperature wet anneals, evinced ordering for all RBS series annealed at 800°C (figure 10b) but no ordering for the 700°C annealed samples.
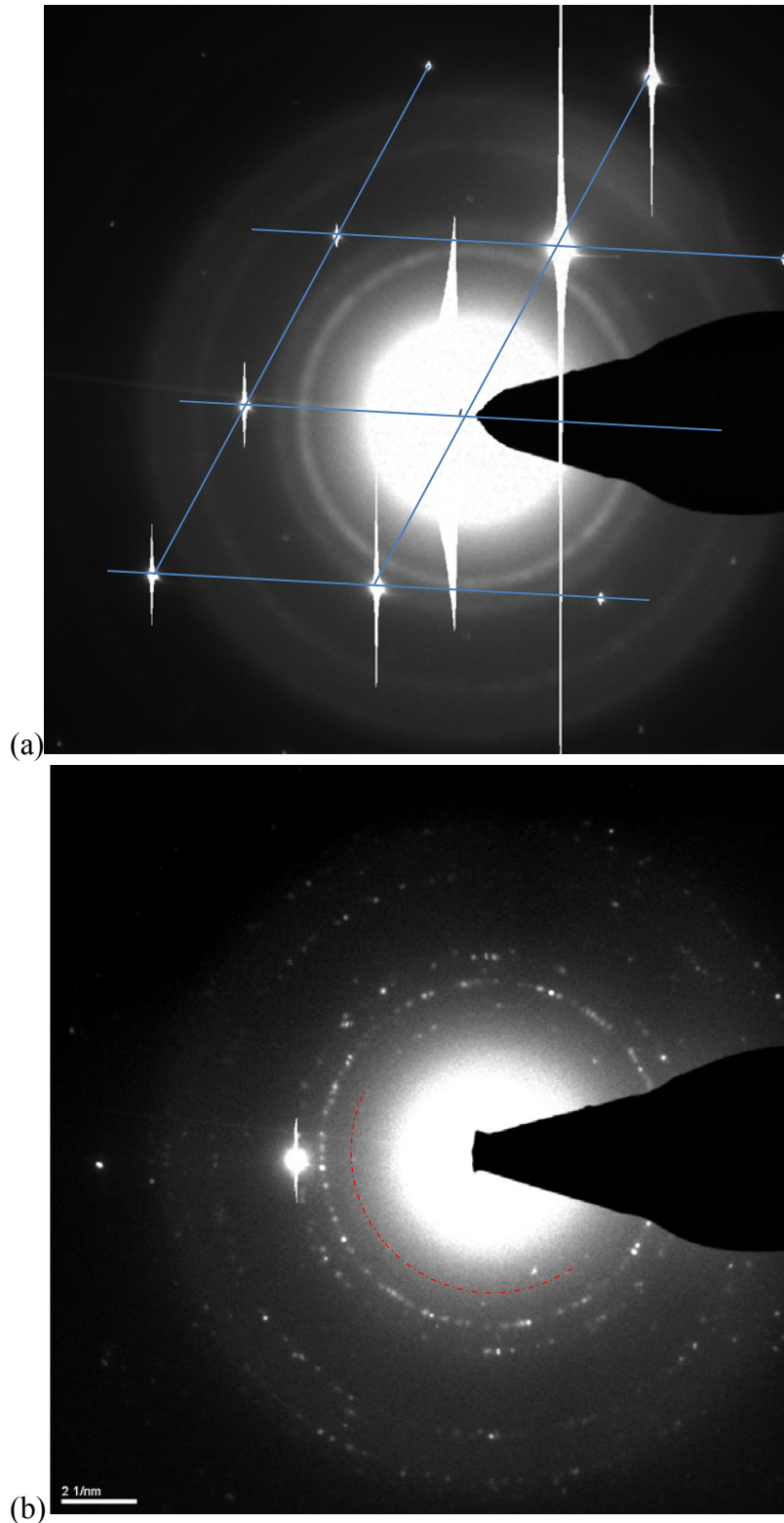
Figure 10: *Fe39Pt10 diffraction patterns from anneals at (a) 600°C, showing Si lattice structure and disordered particles of various orientations; (b) 800°C, showing ordered peaks at the expected radius.*

3.2 EDS Data

As in looking for quality diffraction patterns, the greatest challenge in acquiring EDS

spectra was in finding quality portions of samples to measure. The first samples prepared

(from the 600°C series) each had one or two usable locations at most, so for statistical

rigor, once my sample preparation was more reliable I made new samples from that series

and took new EDS data. Measurements from all sputtering series appeared to have lower

Fe counts than expected, based on the RBS data, and initial analysis confirmed the

samples were too Pt-rich, indicating that the samples might have lost Fe in the annealing

process (figure 11a). At Dr. Vanfleet's suggestion, the higher-temperature samples

requested were performed in a wet anneal environment to prevent Fe diffusion. Spectra

from the later sample set yielded higher Fe counts than in the first set (figure 11b), but

still didn't match the RBS data; considering the known inaccuracy of the default Pt k-

factor, this was expected.

After preliminary analysis of the 800°C anneal samples to correct the Pt k factor,

the 45/10 sample was found to be inconsistent with the other samples, so additional EDS

measurements were made from that same sample. The new measurements matched the

initial measurements. Data was then taken for the unannealed Fe45/Pt10 sample, which

also matched the original measurement.

The expected Co peak from the pole piece in the TEM column was observed in all

EDS measurements, but varied in prominence depending on sample positioning.
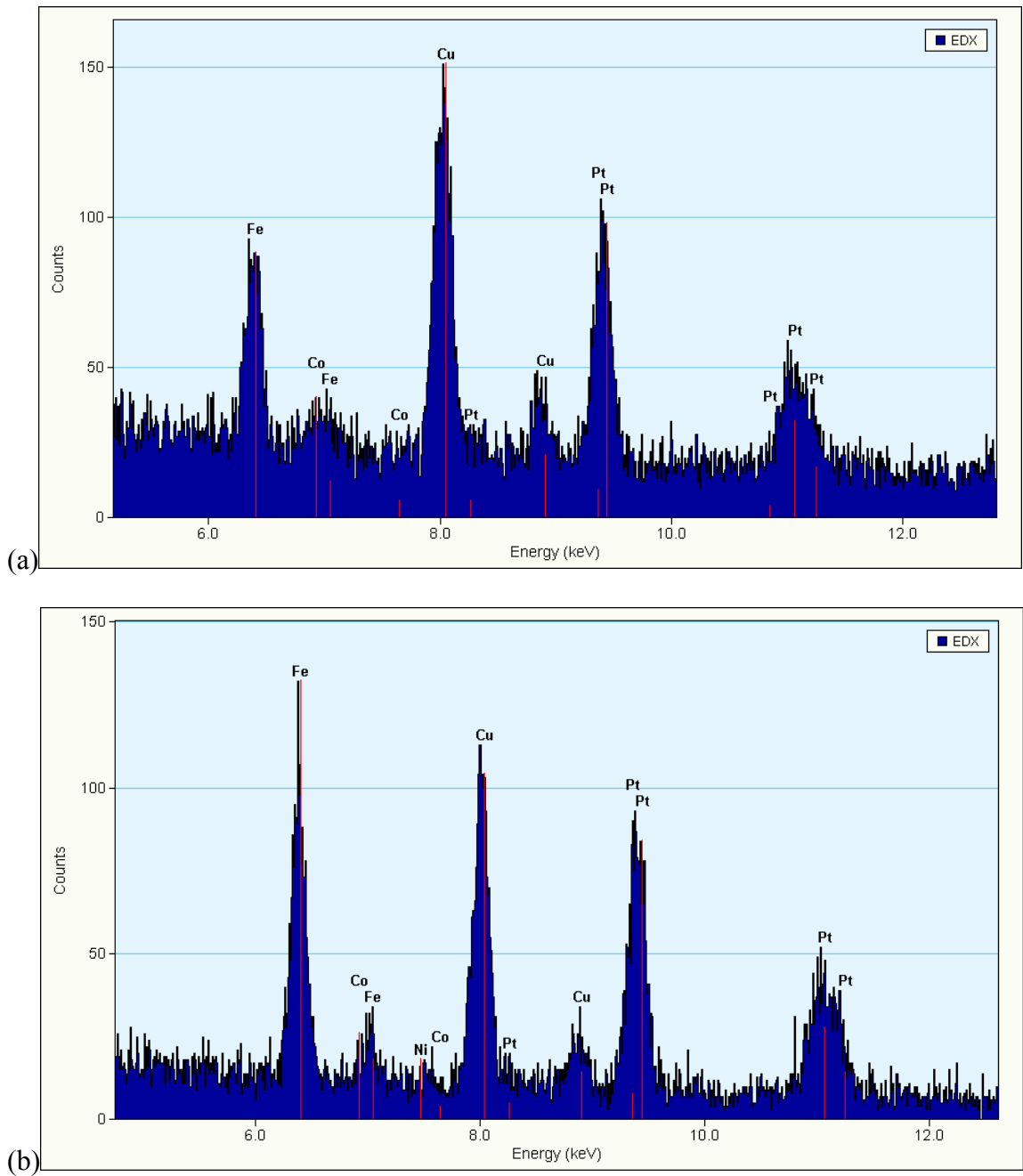
Figure 11: *Raw EDS spectra before analysis, from Fe39Pt10 samples. The Co peak from the pole piece is visible (though not prominent) at 6.9 keV in both samples, as is the central copper peak from the washer the samples are mounted on. (a) In the 600°C anneal, Fe has fewer counts than Pt. (b) In the 800°C anneal, Fe and Pt have more comparable counts.*

CHAPTER 4

Analysis and Discussion

4.1 Impact of anneal conditions

Following the procedure outlined in Section 4.2 for quantification of sample composition and using default *k*-factors, initial EDS analysis of samples from 600°C anneals indicated much lower Fe content in the nanoparticles than expected from the RBS data. Similar Fe deficiency was found in the 500°C and 400°C anneals. Reference to previous work indicated that Fe in the sample could diffuse through the SiO_2 and into the Si substrate during the dry annealing process, yielding samples with a higher Pt content than was desired [6], and rendering the RBS measurements for the 400°C, 500°C, and 600°C anneal samples inaccurate. UCF thus prepared new samples from the same RBS data series processed in a wet anneal instead of a dry anneal.

Comparison of the Fe content of dry-annealed and wet-annealed samples from the same sputtered wafer, with the same RBS composition, revealed a distinct jump in Fe composition from the dry samples to the wet (figure 12). Even recognizing that the default Pt *k*-factor was likely giving inaccurate quantitative results, this observed qualitative difference confirmed that the iron in the sample probably diffused across the SiO_2 substrate layer under the dry anneal conditions, as had been observed in earlier projects. The balance between oxidization and reduction processes when water vapor was present in the wet anneals apparently counteracted this effect. This, in addition to the
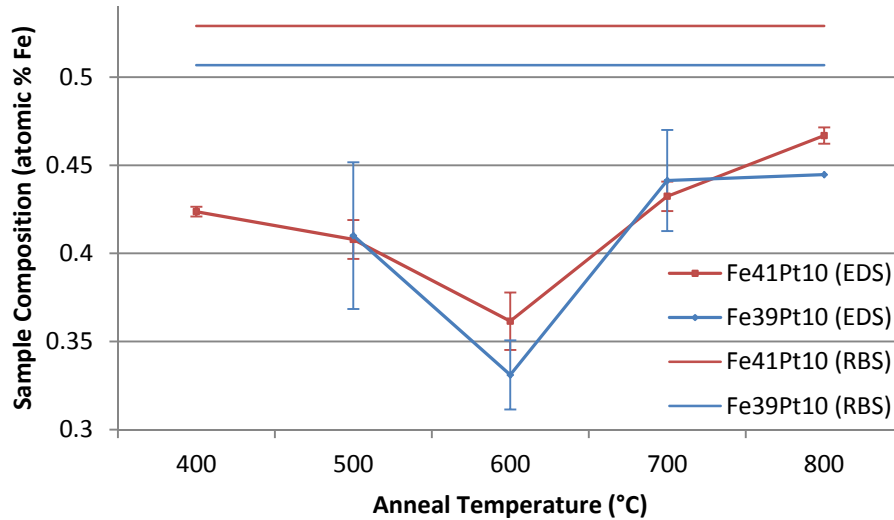
Figure 12: Iron content in dry anneals (400°C, 500°C, 600°C) vs. wet anneals (700°C, 800°C), calculated using ES Vision's default Pt k-factor. In all samples, Fe content is lower than expected on the basis of RBS measurements.

consistency in sample composition between the 700°C and 800°C anneals, and the fact

that the 800°C anneals demonstrated ordering (which would be impossible if they weren't

in the desired range of compositions), indicated that the RBS data for these wet annealed

samples was most likely accurate and could be used as a standard from which to calculate

a *k*-ratio.

4.2 Comparison of EDS and RBS

To quantify the EDS spectra obtained experimentally and convert them into useful data,

the analytic program ES Vision was used. With user input and adjustment, the program

first fits a fifth-degree polynomial to the background count level by imposing background

windows over regions of the spectrum with primarily background contributions (figure

13a). The program next generates a background corrected spectrum, and superposes

Gaussian functions with typical resolutions of 136-150 eV full-width half-maxima to
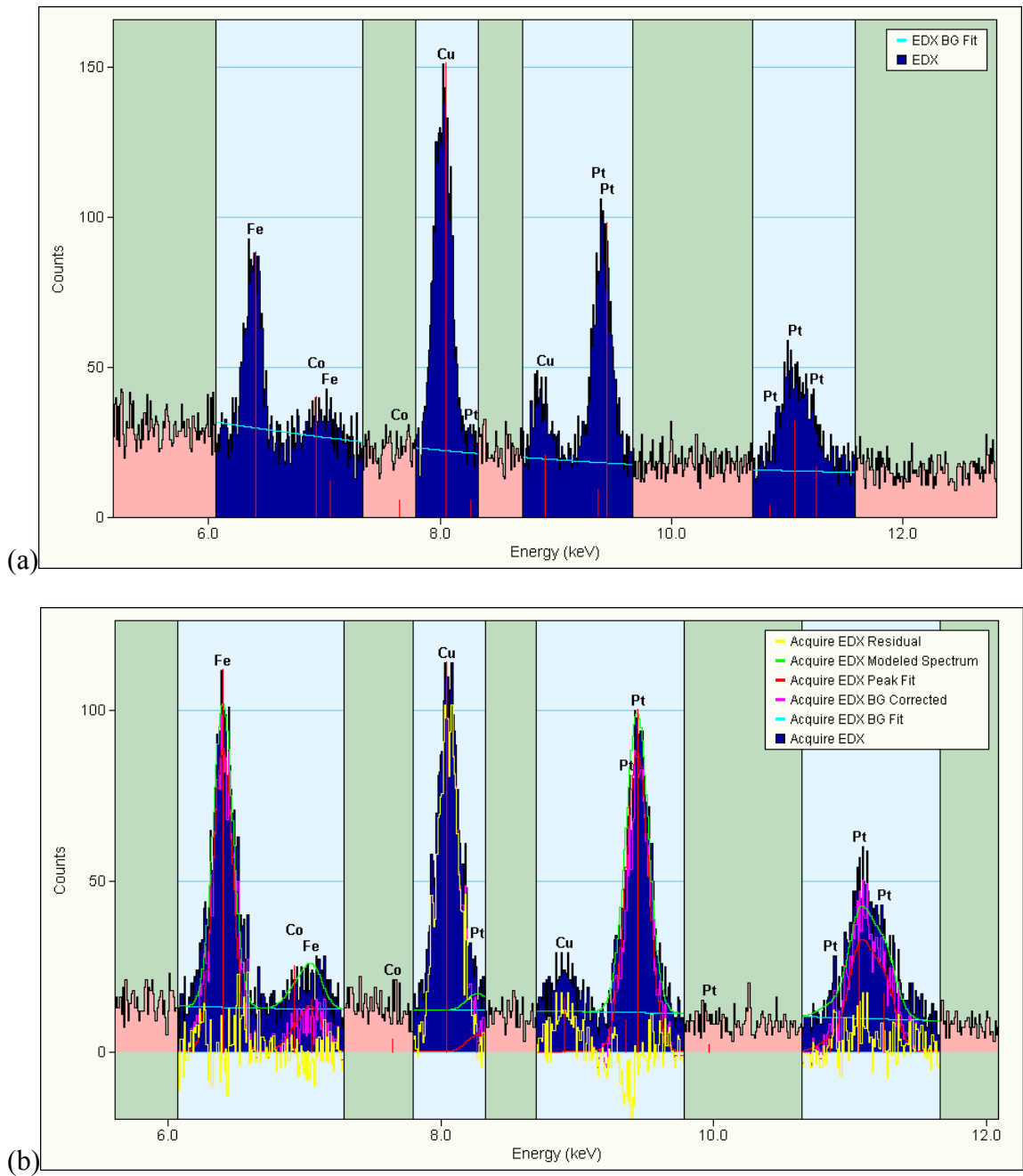
Figure 13: *(a) Fe39Pt10 at 600°C EDS spectrum with background windows (green) and background fit (blue) (b) Fe39Pt10 at 500°C EDS spectrum ready for quantification; the green curve is the modeled Gaussians, the pink represents the background-corrected fit, the yellow indicates residual counts after the background correction and should average around zero if the fit is appropriate.*

model the Fe, Co, and Pt edges. The user adjusts the horizontal axis of the EDS spectrum

so that these Gaussians, centered on the iron K_α-edge at 6.4 keV, the Co K edge at 6.9

keV, and the double platinum L_α-edge at 9.364 and 9.439 keV [7], fit the actual count

data as closely as possible, and successively adjusts both background windows and

horizontal scale until the fit is optimal (figure 13b). The program then integrates the

counts in each peak and automatically calculated the sample's weight and atomic

percentages. This process of analysis yields slightly different integration totals depending

on the background curve and the centering of the Gaussians, so I re-quantified each

spectrum four times and averaged the data from each quantification in calculating overall

values.

After calculating the integrated intensity of each peak, the Cliff-Lorimer

technique is the most common means of relating samples' integrated EDS spectrums to

their chemical compositions by solving the following system of equations:

$$\frac{C_A}{C_B} = k_{AB} \cdot \frac{I_A}{I_B}, \ \frac{C_B}{C_C} = k_{BC} \cdot \frac{I_B}{I_C}, \ \frac{C_A}{C_C} = k_{AC} \cdot \frac{I_A}{I_C}, \ \dots \qquad\qquad 4.1$$

$$C_A + C_B + C_C + \dots = 1 \qquad\qquad 4.2$$

where C_A, C_B, C_C, etc. are the relative compositions of elements A, B, C, etc. in the

sample; I_A, I_B, and I_C are the integrated intensities (number of counts) of each element's

K or L edge from the EDS spectrum, and k_{AB}, k_{BC} etc. are the ratios between the k-factors

for elements A, B, and C, i.e. $k_{AC} = \frac{k_A}{k_C}$. The k-factors themselves depend on the specific

experimental apparatus; there are correction factors for detector efficiency at specific

energies, and each k-factor is calibrated relative to a standard (for this system Si) which

has a k-factor defined to be 1. For a sample with only two elements (for this research Fe

and Pt), let $k_{AB} \cdot \frac{I_A}{I_B} = \alpha$ so that equation 4.1 becomes $C_A = \alpha \cdot C_B$ and equation 4.2 yields

$$C_B = \frac{1}{1+\alpha}.$$
4.3

For three elements (in this research Fe, Pt, and Co), $k_{AC} \cdot \frac{I_A}{I_C} = \alpha$ and $k_{BC} \cdot \frac{I_B}{I_C} = \beta$ and

thus $C_A = \alpha \cdot C_C$, $C_B = \beta \cdot C_C$ giving

$$C_C = \frac{1}{1+\alpha+\beta}.$$
4.4

The Cliff-Lorimer technique can be used to calculate chemical compositions by weight percentage or by atomic percentage; the only difference in the values of the *k*-factors used, since heavier atoms (like Pt) will interact more with the electron beam than lighter atoms (like Fe). Since $L1_0$ ordering depends on having equal numbers of Fe and Pt atoms to occupy the lattice sites, atomic percent composition is the value of interest to this research, and the RBS data is given in atomic percent, but ES Vision by default uses weight-calibrated *k*-factors. To convert from weight composition to atomic composition, the calculated *C*s are just scaled by the ratio between the atomic masses:

$$\frac{C_A}{C_B} = \frac{N_A}{N_B} \cdot \frac{A_A}{A_B} \quad \rightarrow \quad \frac{N_A}{N_B} = \frac{C_A}{C_B} \cdot \frac{A_B}{A_A}, \quad \dots$$
4.5

where N_A, N_B etc. are the atomic percent compositions (which also satisfy eq. 4.2) and A_A, A_B etc. are the atomic masses (Fe: 55.845 amu, Co: 58.933 amu, Pt: 195.078 amu).

To take the RBS measurements as a standard and experimentally obtain a new k_{Pt} I must first obtain the ratio between the atomic *k*-factors for Fe and Pt, which is simply obtained by substituting the RBS *N*s for the *C*s in the Cliff-Lorimer technique:

$$\frac{N_A}{N_B} = k'_{AB} \cdot \frac{I_A}{I_B} \quad \rightarrow \quad k'_{AB} = \frac{N_A}{N_B} \cdot \frac{I_B}{I_A}$$
4.6

where k' indicates calibration for atomic, not weight, composition.

Next, substituting eq. 4.1 into eq. 4.3 and setting it equal to eq. 4.4, the integrated intensities cancel and the following expression for the new Pt weight percent k-factor is obtained:

$$\frac{N_A}{N_B} = \frac{C_A}{C_B} \cdot \frac{A_B}{A_A} = \frac{k_A}{k_B} \cdot \frac{I_A}{I_B} \cdot \frac{A_B}{A_A} = k'_{AB} \cdot \frac{I_A}{I_B} \qquad 4.7$$

$$\rightarrow k_A = k_B \cdot k'_{AB} \cdot \frac{A_A}{A_B} \qquad 4.8$$

I can either presume that the FeCo pole piece did not contribute significantly to the Fe counts, and carry out all of these calculations simply with Pt as element A and Fe as element B, or compensate for the pole piece by adding a third element (Co as element C) to the system of equations. In compensating for the pole piece (which I presume to be 50% Fe), since Fe and Co have comparable atomic weights and are chemically very similar (atomic numbers 26 and 27 respectively) I can simply subtract the integrated number of Co counts from the integrated number of Fe counts and use that reduced number in calculations. If the other metal in the pole piece were more dissimilar to Fe, however, I would need to calculate its atomic percent composition, subtract that from iron's atomic percent composition, and re-scale the Fe and Pt compositions by equation 4.2. Both methods are represented in the spreadsheet provided in Appendix 1.

The Co-corrected calculations yield rather different values than were obtained by simple FePt count analysis, as shown in figure 14. For experimental rigor, and since the data seems more coherent with the Co correction, I use the results of the Co-corrected calculations for my experimental conclusions.
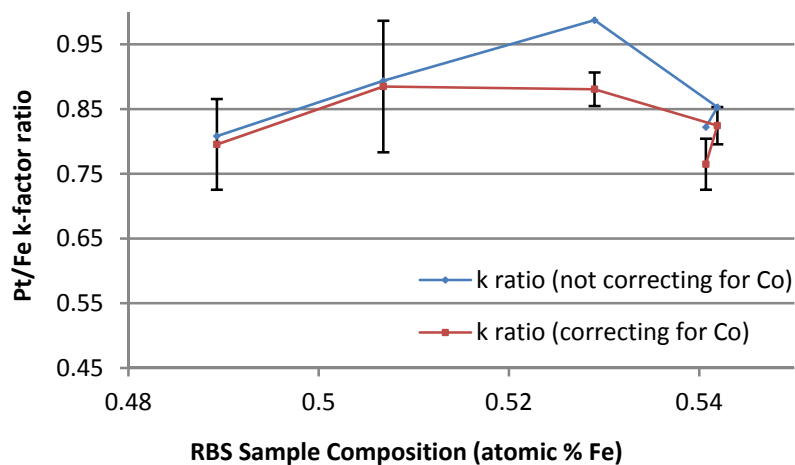
Figure 14: *Calculated k-ratios for each of the five samples annealed at 800C*

As has been mentioned previously, at least four EDS spectra were taken from each sample, and each spectrum was quantified four times. Thus, the counts from all of those quantifications (16 or more per sample) were entered into an Excel spreadsheet with these equations to calculate an atomic average *k*-ratio (eq. 4.6) between Fe and Pt *k*-factors for each sample. These sample average *k*-ratios were then averaged, yielding an overall atomic *k*-ratio of 0.83 ± 0.05 for this research.

To calculate the specific Pt *k*-factor, the average atomic *k*-ratio of each individual sample was used in eq. 4.7 to find the weight percent *k*-factor of that sample, with the five *k*-factors averaged for a Pt L edge weight percentage *k*-factor of 4.291 ± 0.272.

Using this *k*-factor instead of ES Vision's default value to re-analyze the EDS spectra from figure 12 yields much better agreement with the RBS measurements than the default *k*-factor (figure 15), and also allows for a definitive measurement of how much Fe was lost in the dry anneals; at 400°C about 3% is lost, but that increases to ~10% for both series at 600°C.
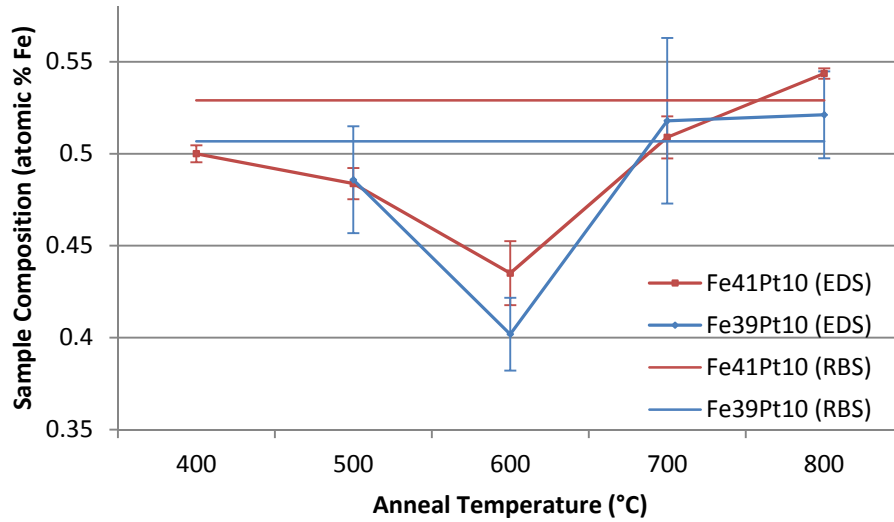
Figure 15: *The newly determined* k*-factor gives re-calculated sample compositions that agree much better with RBS measurements, with expected Fe-deficiency in the dry anneals.*

4.3 Validity of RBS Measurements

Following the procedure outlined above yielded *k*-ratios for four of the samples within a margin of error from one another (when correcting for the FeCo pole piece), and one *k*-ratio outlier: the sample sputtered at 45 W Fe (see figure 16). To verify that the data from the 45/10 sample wasn't faulty, I took new EDS spectra from that same sample to re-
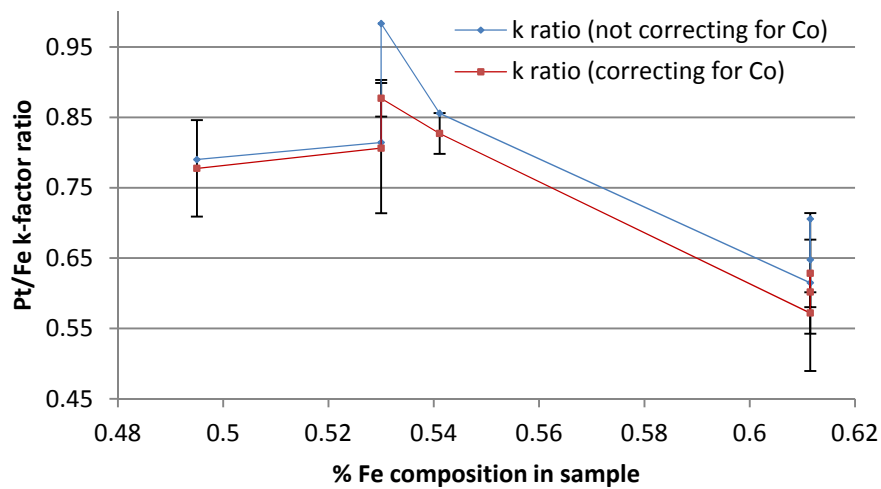
Figure 16: *Initial graph of calculated* k*-factors for samples by RBS composition*

calculate the *k*-ratio, and also prepared and analyzed an unannealed sample from the 45/10 sputtering series for comparison; both yielded k-ratios which were considerably closer to the originally calculated 45/10 k-ratio than to the k-ratios of the other samples (figure 16). While this served to verify that my quantification of the 45/10 series was accurate, it brought into question the validity of the RBS value for those samples. Redoing the RBS measurement of that sample yielded a very different composition (lower by over 8%), bringing into question the validity of all of the original RBS values. Redoing all of the RBS measurements confirmed that the 37/10, 39/10, 41/10, and 43/10 RBS data was fairly accurate, as was the second value for the 45/10 sample (table 1).

For the sake of consistency, the third set of RBS measurements was used as the standard from which the *k*-ratios and *k*-factors in section 4.2 were obtained. EDS measurements of the series annealed at 800°C were used, and as shown in Table 1, generally agree with the RBS measurements.

Fe/Pt sputtering power	Fe atomic composition				
	RBS (1st set)	RBS (2nd set)	RBS (3rd set)	EDS (default *k*)	EDS (new *k*)
37/10	0.495	-	0.4893	.4101	.4758
39/10	0.53	-	0.5068	.4447	.5212
41/10	0.53	-	0.529	.4668	.5095
43/10	0.5411	-	0.5419	.4633	.5059
45/10	0.6115	0.5301	0.5407	.4435	.4859

Table 1: *RBS and EDS measurements of sample compositions*

4.4 Discussion of error

The primary three sources of potential experimental error in this research were inaccuracy of sample processing, inaccuracy of RBS measurements and analysis, and inaccuracy of EDS measurements and analysis.

Sample processing through sputtering, annealing and polishing could contribute to experimental error. In the sputtering process, it is possible that certain regions of the deposited alloys had higher Fe content than other regions; this regional variation could account for some of the discrepancies between EDS measurements on the same sample and contribute to uncertainty in the averaged values. The potential for anneal conditions to change sample composition from measured values was addressed in section 4.1; in the dry anneals, higher temperatures were definitively linked with increased Fe loss. While there is reason to believe that adding water vapor to the anneal environment solved the problem of Fe attrition in the samples used to obtain the experimental results (the 800°C anneals) it is possible that some smaller amount of Fe was still lost. Determining the extent of that effect could have been accomplished by analyzing as-deposited samples and comparing them with their annealed counterparts, and this was carried out for the 45/10 samples. In that instance, the difference seemed to be negligible (within 3%), so due to time constraints the other sputtering series did not undergo similar analysis and comparison. The colloidal silica phase of sample polishing has the potential to impact the experiment either through residual colloidal silica interfering with EDS measurement accuracy or through etching the outer surface of the particles. These effects were minimized by taking spectra only from sample regions which were free of colloidal silica when possible.

Obtaining two RBS measurements for four of the sample sputtering series and three measurements for a fifth confirmed the general accuracy of those measurements; the first measurement for the 45/10 samples was a clear aberration, and the third set of requested data matched previous values to within 3% (see table 1). Two data points isn't the most ideal sample size for statistical confidence, but was sufficient for the purposes of this research.

EDS quantification can be inaccurate if the energy edges are insufficiently distinct from the background, but using the methods described in section 2.4 ensured that only higher-quality spectra were included in analysis. The EDS measurements used in this project had limited energy resolution, which could have presented difficulties in terms of getting accurate counts for the K and L edges if the peaks of interest were more closely-spaced, but since the Fe K edge and Pt L edge are energetically far enough apart there, was no difficulty from that sector. The default calculation method for EDS analysis is known to be inaccurate; the object of this research was to reduce that error by calculating a new *k*-factor which can be used to calculate sample compositions with greater accuracy and confidence, and this goal was reached.

CHAPTER 5

Conclusion

5.1 *k* factor confidence

It can be difficult to verify the quality of experimentally obtained constants without either comparison against external standards or extensive testing. The Pt L-edge *k*-factor obtained in the course of this research (4.291) differs significantly from my only standard of comparison, the *k*-factor which the manufacturer of BYU's EDS detector provided (5.838). Yet, as a matter of interest, the BYU microscopy facility underwent an upgrade between the time that I began obtaining and analyzing the data for this thesis and the submission deadline. As part of the upgrade, the ES Vision software which accompanies the EDAX system was updated to a newer version, as was its database of *k*-factors. In the new database, the Pt L-edge *k*-factor is 4.176. That the manufacturer independently re-calculated the *k*-factor and arrived at a value within the margin of error of my calculated value gives great confidence to the integrity of my experimental value.

The manufacturer's provided value is an estimate based on theoretical models which don't wholly incorporate all the factors involved in actual experimental apparatus. Thus, considering that each individual experimental set-up by nature has a slightly different actual *k*-factor, the experimental value obtained in the course of this research is preferable to the manufacturer value for use in research conducted at BYU, as this value has been specifically calculated for this system.

5.2 Implications for further research

The experimentally determined Pt *k*-factor will enable improved accuracy in EDS analysis here at BYU, which can be beneficial to many different projects here at BYU, since EDS is a frequently used feature of this TEM system, and Pt is a common material of study not only in nanoparticles but also in thin films and other areas of research.

Mapping the order-disorder transition of particles over a range of compositions is the eventual goal of this type of research; thus, this more accurate method for determining the composition of specific particles will enable researchers to correlate the order-disorder temperature of a particle with its composition and potentially generate a phase diagram of the type provided in Figure 1. Specifically, as research into the order-disorder transition behavior of bimetallic nanoparticles continues, the Pt *k*-factor calculated here will be of great benefit in tracking the behavior of NiFePt nanoparticles. Since the transition temperature for FePt nanoparticles is likely out of the range of BYU's experimental apparatus (which only goes to ~1000°C), while NiPt doesn't have sufficient driving force to order at anneal temperatures, the pseudo-bimetallic alloy NiFePt should have both strong ordering at anneal temperatures and a reasonably low transition temperature. With three elements in the nanoparticles, accurate composition analysis will be even more important, and preliminary use of the *k*-factor obtained in this thesis has already proved beneficial to researchers working with those nanoparticles.

References

[1] B. Yang, M. Asta, O.N. Mryasov, T.J. Klemmer, R.W. Chantrell, "The Nature of A1-L10 ordering transitions in alloy nanoparticles: A Monte Carlo study", Acta materialia 54 (2006) 4201-4211.

[2] K.H.J. Buschow (ed) 2011. *Handbook of Magnetic Materials, Vol. 19*. Elsevier 2011.

[3] C. Rong, D. Li, V. Nandwana, N. Poudyal, Y. Ding, Z. Lin Wang, H. Zeng, and J. Ping Liu, "Size-Dependent Chemical and Magnetic Ordering in L10-FePt Nanoparticles" Advanced Materials 18 (2006): 2984–2988

[4] Massalski, T. B., .Binary Alloy Phase Diagrams, 2nd edition, ASM International, Materials Park OH, 1990.

[5] Williams, D.B., 2004. *Transmission Electron Microscopy: A Textbook for Materials Science, Vol. IV: Spectrometry.* Springer.

[6] B. Yao, R. V. Petrova, R. R. Vanfleet, K. R. Coffey, "Compositional Stability of FePt Nanoparticles on SiO2/Si During Annealing," Journal of Applied Physics 99 (8): Art. No. 08E913 APR 15 2006.

[7] Laby, T.H., 1995. *Tables of physical and chemical constants, 16th edition (online version).* Longman science and technology. Accessed at http://www.kayelaby.npl.co.uk/atomic_and_nuclear_physics/4_2/4_2_1.html

Appendix 1

An example of the spreadsheets used in the analysis from section 4.2:

	Detector Correction	Default k-factor	Atomic Mass
Fe (K edge)	0.994	1.48	55.845
Co (K edge)	0.995	1.576	58.9332
Pt (L edge)	0.752	5.838	195.078

RBS atomic composition

Fe	0.4893
Pt	0.5107

EDS Composition

Fe	40.39%	0.021719
Pt	59.61%	

Element	Counts (I)	Error	Weight (C)	Atomic (N)	Error		Count Ratio	Eq. 4.8		Count ratio	× k-ratio	Weight %	Atomic %	Correct from Co	Normalize	Ignoring Co	Co-corrected	k-factor

Calculated Composition (Default) | Method 1 | Method 2 | Atomic k-ratio (Pt/Fe) Eq. 4.6 | k-factor Eq 4.8

Fe37Pt10 800 C\04_edx.emi

Fe (K edge)	1645.68	383.155	17.691	42.884	0.41	Fe'=Fe-Co	1645.68	4.573687	Co/Fe	0	0	17.69%	42.88%	42.88%	42.88%	0.885	0.885	4.573687
Co (K edge)	0	100	0	0	100				Co/Fe			0.00%	0.00%	0.00%				
Pt (L edge)	1941.58	383.939	82.308	57.115	1.439	Pt/Fe'	1.179804093	4.573687	Pt/Fe	1.179804093	4.653849	82.31%	57.12%	133.23%	57.12%			

Fe (K edge)	1630.096	381.419	17.746	42.978	0.413	Fe'	1630.096	4.591116	Co/Fe	0	0	17.74%	42.97%	42.97%	42.97%	0.888	0.888	4.591116
Co (K edge)	0	100	0	0	100				Co/Fe			0.00%	0.00%	0.00%				
Pt (L edge)	1915.893	338.521	82.253	57.021	1.448	Pt/Fe'	1.175325257	4.591116	Pt/Fe	1.175325257	4.636182	82.26%	57.03%	132.72%	57.03%			

Fe (K edge)	1636.144	384.253	18.537	44.26	0.434	Fe'	1633.024	4.835076	Co/Fe	0.001906923	0.002031	18.53%	44.25%	44.17%	44.24%	0.937014983	0.935211972	4.834992
Co (K edge)	3.12	88.534	0.037	0.085	0.106				Co/Fe			0.04%	0.09%	0.19%				
Pt (L edge)	1822.492	330.171	81.425	55.654	1.473	Pt/Fe'	1.11602279	4.835076	Pt/Fe	1.113894621	4.393863	81.43%	55.66%	125.78%	55.76%			

Fe (K edge)	1641.039	382.207	18.057	43.497	0.419	Fe'	1641.039	4.689329	Co/Fe	0	0	18.05%	43.49%	43.49%	43.49%	0.907036956	0.907036956	4.689329
Co (K edge)	0	100	0	0	100				Co/Fe			0.00%	0.00%	0.00%				
Pt (L edge)	1888.359	336.289	81.942	56.502	1.455	Pt/Fe'	1.150709398	4.689329	Pt/Fe	1.150709398	4.539082	81.95%	56.51%	129.94%	56.51%			

Fe37Pt10 800 C\05_edx.emi

Fe (K edge)	1417.262	361.658	15.762	39.217	0.4	Fe'	1376.914		Co/Fe	0.028468978	0.030316	15.76%	39.21%	38.08%	38.96%	0.774575599	0.752324347	3.889474
Co (K edge)	40.348	102.021	0.477	1.126	0.12				Co/Fe			0.48%	1.13%	2.87%				
Pt (L edge)	1909.752	337.266	83.759	59.655	1.473	Pt/Fe'	1.386979869	3.890507	Pt/Fe	1.347493971	5.315317	83.76%	59.66%	152.16%	61.04%			

Fe (K edge)	1380.832	356.913	15.239	38.337	0.392	Fe'	1348.879		Co/Fe	0.023140397	0.024641	15.24%	38.33%	37.44%	38.12%	0.743333857	0.725976904	3.753259
Co (K edge)	31.953	97.373	0.375	0.895	0.114				Co/Fe			0.38%	0.90%	2.34%				
Pt (L edge)	1938.865	338.747	84.384	60.767	1.469	Pt/Fe'	1.437389862	3.754065	Pt/Fe	1.404128091	5.538716	84.39%	60.77%	158.56%	61.88%			

Fe (K edge)	1361.464	356.939	15.147	38.094	0.392	Fe'	1319.949		Co/Fe	0.030492911	0.032471	15.14%	38.09%	36.91%	37.80%	0.73902145	0.716282276	3.703138
Co (K edge)	41.515	102.985	0.491	1.172	0.12				Co/Fe			0.49%	1.17%	3.08%				
Pt (L edge)	1922.825	340.361	84.36	60.733	1.476	Pt/Fe'	1.456741889	3.704194	Pt/Fe	1.412321589	5.571036	84.36%	60.74%	159.48%	62.20%			

Fe (K edge)	1401.763	360.066	15.401	38.588	0.394	Fe'	1363.873		Co/Fe	0.027030247	0.028784	15.40%	38.58%	37.53%	38.34%	0.753251457	0.732706333	3.78805
Co (K edge)	37.89	100.576	0.443	1.052	0.117				Co/Fe			0.44%	1.05%	2.73%				
Pt (L edge)	1942.34	339.263	84.155	60.359	1.464	Pt/Fe'	1.424135532	3.789004	Pt/Fe	1.385640797	5.465791	84.16%	60.37%	156.47%	61.66%			

Fe37Pt10 800 C\06_edx.emi

Fe (K edge)	1926.438	423.52	17.815	42.872	0.386	Fe'	1893.678		Co/Fe	0.017005479	0.018109	17.81%	42.86%	42.13%	42.76%	0.895746755	0.880376083	4.551494
Co (K edge)	32.76	100.392	0.322	0.735	0.097				Co/Fe			0.32%	0.74%	1.72%				
Pt (L edge)	2244.711	368.348	81.861	56.392	1.325	Pt/Fe'	1.185371008	4.552208	Pt/Fe	1.165213207	4.596294	81.87%	56.40%	131.58%	57.24%			

Fe (K edge)	1893.572	416.808	16.728	41.017	0.366	Fe'	1858.639		Co/Fe	0.018448203	0.019645	16.72%	41.01%	40.25%	40.87%	0.830110081	0.814657233	4.211731
Co (K edge)	34.933	101.496	0.328	0.763	0.095				Co/Fe			0.33%	0.76%	1.86%				
Pt (L edge)	2380.876	373.176	82.943	58.218	1.294	Pt/Fe'	1.280978178	4.212449	Pt/Fe	1.257346433	4.959722	82.95%	58.23%	141.98%	59.13%			

Fe (K edge)	1941.636	421.796	16.866	41.326	0.364	Fe'	1917.518		Co/Fe	0.012421484	0.013227	16.86%	41.32%	40.80%	41.23%	0.83727596	0.826781482	4.274413
Co (K edge)	24.118	94.847	0.223	0.518	0.087				Co/Fe			0.22%	0.52%	1.25%				
Pt (L edge)	2420.415	378.611	82.91	58.155	1.29	Pt/Fe'	1.262264552	4.2749	Pt/Fe	1.246585354	4.917274	82.91%	58.16%	140.77%	58.77%			

Fe (K edge)	1949.218	422.385	16.828	41.252	0.363	Fe'	1923.444		Co/Fe	0.013222739	0.01408	16.82%	41.25%	40.69%	41.15%	0.835185685	0.824042144	4.260251
Co (K edge)	25.774	95.999	0.237	0.55	0.087				Co/Fe			0.24%	0.55%	1.33%				
Pt (L edge)	2435.948	378.277	82.934	58.196	1.282	Pt/Fe'	1.26645122	4.260768	Pt/Fe	1.249705266	4.929581	82.94%	58.20%	141.12%	58.85%			

Fe37Pt10 800 C\07_edx.emi

Fe (K edge)	1508.832	37.866	16.874	41.477	0.412	Fe'	1507.194		Co/Fe	0.001085608	0.001156	16.87%	41.47%	41.42%	41.46%	0.835708801	0.834793325	4.315834
Co (K edge)	1.638	87.822	0.019	0.045	0.104				Co/Fe			0.02%	0.05%	0.11%				
Pt (L edge)	1884.415	335.694	83.106	58.477	1.473	Pt/Fe'	1.250280322	4.315876	Pt/Fe	1.248923008	4.926495	83.11%	58.48%	141.03%	58.54%			

Fe (K edge)	1501.872	370.646	16.193	40.286	0.396	Fe'			Co/Fe	0.000964796	0.001027	16.19%	40.28%	40.24%	40.27%	0.79544005	0.794665656	4.108376
Co (K edge)	1.449	86.967	0.016	0.039	0.099				Co/Fe			0.02%	0.04%	0.10%				
Pt (L edge)	1970.68	341.412	83.789	59.673	1.441	Pt/Fe'	1.313416283	4.108412	Pt/Fe	1.312149105	5.175896	83.79%	59.68%	148.17%	59.73%			

Fe (K edge)	1521.311	372.042	16.832	41.361	0.409	Fe'	1514.115		Co/Fe	0.004730131	0.005037	16.83%	41.35%	41.16%	41.32%	0.833879669	0.829899556	4.290533
Co (K edge)	7.196	87.719	0.084	0.197	0.102				Co/Fe			0.08%	0.20%	0.48%				
Pt (L edge)	1904.168	335.337	83.082	58.441	1.457	Pt/Fe'	1.257611212	4.290718	Pt/Fe	1.251662546	4.937301	83.09%	58.45%	141.34%	58.68%			

Fe (K edge)	1499.965	369.746	16.209	40.287	0.397	Fe'	1494.845		Co/Fe	0.003413413	0.003635	16.21%	40.28%	40.14%	40.25%	0.796799804	0.794055344	4.10522
Co (K edge)	5.12	88.618	0.058	0.138	0.101				Co/Fe			0.06%	0.14%	0.34%				
Pt (L edge)	1964.819	340.4	83.731	59.573	1.443	Pt/Fe'	1.314396476	4.105348	Pt/Fe	1.309909898	5.167064	83.74%	59.58%	147.92%	59.75%			

Fe37Pt10 800 C\08_edx.emi

Fe (K edge)	1238.166	335.299	14.637	37.462	0.394	Fe'	1238.166		Co/Fe	0	0	14.63%	37.45%	37.45%	37.45%	0.705794976	0.705794976	3.648919
Co (K edge)	0	100	0	0	100				Co/Fe			0.00%	0.00%	0.00%				
Pt (L edge)	1831.011	330.502	85.362	62.537	1.531	Pt/Fe'	1.47880898	3.648919	Pt/Fe	1.47880898	5.833302	85.37%	62.55%	166.99%	62.55%			

Fe (K edge)	1334.441	346.405	15.038	38.208	0.388	Fe'	1334.441		Co/Fe	0	0	15.03%	38.20%	38.20%	38.20%	0.728544685	0.728544685	3.766534
Co (K edge)	0	100	0	0	100				Co/Fe			0.00%	0.00%	0.00%				
Pt (L edge)	1911.762	336.101	84.961	61.791	1.487	Pt/Fe'	1.432631342	3.766534	Pt/Fe	1.432631342	5.65115	84.97%	61.80%	161.78%	61.80%			

Fe (K edge)	1307.434	342.796	15.088	38.299	0.394	Fe'	1307.434		Co/Fe	0	0	15.08%	38.29%	38.29%	38.29%	0.73136497	0.73136497	3.781115
Co (K edge)	0	100	0	0	100				Co/Fe			0.00%	0.00%	0.00%				
Pt (L edge)	1865.848	331.946	84.911	61.7	1.505	Pt/Fe'	1.427106837	3.781115	Pt/Fe	1.427106837	5.629358	84.92%	61.71%	161.15%	61.71%			

Fe (K edge)	1291.318	340.299	14.769	37.707	0.388	Fe'	1291.318		Co/Fe	0	0	14.77%	37.70%	37.70%	37.70%	0.713223211	0.713223211	3.687323
Co (K edge)	0	100	0	0	100				Co/Fe			0.00%	0.00%	0.00%				
Pt (L edge)	1889.724	333.383	85.23	62.292	1.501	Pt/Fe'	1.463407155	3.687323	Pt/Fe	1.463407155	5.772548	85.23%	62.30%	165.25%	62.30%			

Average k-factor 4.141577
Standard Deviation 0.375492

Average k-ratio: 0.808   0.795
Standard Deviation: 0.068576052   0.070101992

Average k-factor 4.141239
Standard Deviation 0.375606

Appendix 2

All raw EDS and diffraction data used in this thesis, as well as additional TEM images,

EDS spectra, and diffraction images, can be found on the enclosed CD-Rom.